AD-A194 214 THE NBS/NRL (NATIONAL BUREAU OF STANDARDS/NAVAL RESEARCH LABORATORY) FREE.. (U) NATIONAL BUREAU OF STANDARDS GAITHERSBURG MD S PENNER ET AL. 1987 1/1

UNCLASSIFIED N00014-87-F-0066 F/G 9/3 NL

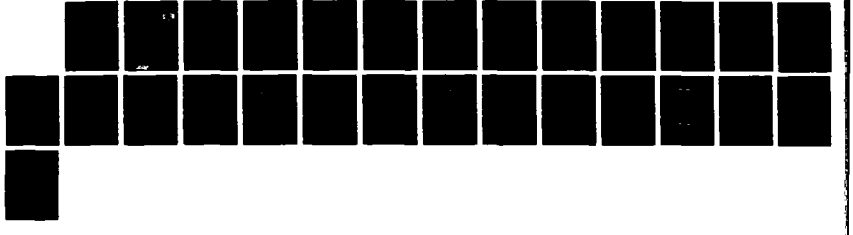

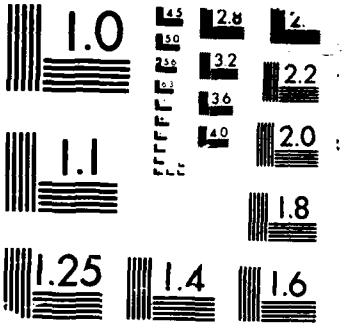

MICROCOPY RESOLUTION TEST CHART

The NBS/NRL FREE ELECTRON LASER FACILITY*

S. Penner, R. Ayres, R. Cutler, P. Debenham, B.C. Johnson,
E. Lindstrom, D. Mohr, J. Rose, and M. Wilson
National Bureau of Standards
Gaithersburg, MD 20899

P. Sprangle and C.M. Tang
Naval Research Laboratory
Washington, DC 20375-5000

Abstract

A free electron laser is being built at the National Bureau of Standards, as a joint project with the Naval Research Laboratory. The electron beam source is the 185-MeV CW racetrack microtron (RTM) presently nearing completion. This accelerator is characterized by extremely good emittance ($\varepsilon_n \lesssim 10$ μm) and small energy spread ($\frac{\Delta\gamma}{\gamma} \lesssim 3 \times 10^{-4}$ at full energy). A new photocathode injector operating on the 32nd subharmonic of the 2380-MHz RF frequency is being developed to increase the peak current to $\gtrsim 2$ A in 3-ps micropulses. Our wiggler design has 130 periods of $\lambda_w = 28$ mm with RMS wiggler parameter $K \lesssim 1$. Three-dimensional calculations indicated that power gains of 10-30% per pass can be achieved for optical wavelengths in the range 200 nm to 10.0 μm. The design of the RTM and FEL will be described. This FEL is intended for use in a broad program of research applications in biomedicine and materials science.

Introduction

An FEL facility is being built at the National Bureau of Standards for research applications in biomedicine, materials sciences, and basic physics and chemistry. The driving accelerator is a 185-MeV CW racetrack microtron (RTM) now nearing completion.

*This work funded by SDIO through ONR Contract No. N00014-87-F-0066.

A CW RTM makes a good driver for a short wavelength FEL because of its excellent beam quality. One condition on the transverse normalized emittance, ε_n, is

$$\frac{\pi\varepsilon_n}{\gamma} \lesssim \lambda \qquad (1)$$

where λ is the optical wavelength of the FEL, and γ is the electron beam energy in units of the electron rest energy, mc^2. [We use $\varepsilon_n = 4\beta\gamma[\langle x^2\rangle\langle x'^2\rangle - \langle xx'\rangle^2]^{1/2}$, where β is the electron velocity in units of c, x and x' are the transverse coordinate and angle to the propagation direction and $\langle\rangle$ signifies average over the beam electrons.] For our 185-MeV machine with the expected value $\varepsilon_n \lesssim 10$ μm, the minimum wavelength according to eq. (1) is $\lambda = 90$ nm. We do not expect to lase on the fundamental below about 200 nm because of the rapidly decreasing gain at shorter wavelength. It may also be possible to lase on the third harmonic down to about 150 nm, the shortest wavelength at which high reflectivity mirrors are available.

The expected good energy spread, $\frac{\Delta\gamma}{\gamma}$, of the RTM is consistent with the long wiggler needed to achieve lasing at short wavelengths. The requirement is

$$\frac{\Delta\gamma}{\gamma} \lesssim \frac{1}{2N} \qquad (2)$$

where N is the number of wiggler periods. Our design calls for N = 130, i.e. $\frac{1}{2N} = 3.8 \times 10^{-3}$, whereas the observed energy spread from the RTM injector at 5 MeV is $\frac{\Delta\gamma}{\gamma} = 1 \times 10^{-3}$. The fractional energy spread is expected to decrease substantially with further acceleration. The small energy spread is particularly important for lasing on the third harmonic and for enhancing the spontaneous coherent emission at higher harmonics.

Accelerator

The electron accelerator of the NBS/NRL FEL facility is the NBS/Los Alamos Racetrack Microtron (RTM). A general description of the RTM is given in reference 1. The machine is scheduled for completion in 1989. Table I lists the design parameters of the RTM, along with the recently-measured performance[2] of the 5-MeV CW injector linac.

Table I

NBS/LOS ALAMOS CW RTM PARAMETERS

	Design	Observed
Injection energy (MeV)	5	5.5
Energy gain per pass, ΔV (MeV)	12	
Number of passes	15	
Maximum energy (MeV)	185	
Maximum current (μA)	550	630 @ 5 MeV
Macroscopic duty factor	100%	
RF frequency (MHz)	2380	
RF wavelength (cm)	12.596	
ε_n (μm)*	< 10	0.7 @ 5 MeV
Longitudinal emittance, ε_Z (keV-degrees)	< 30	< 5 @ 5 MeV

*See definition in text

In order to increase the FEL gain, it will be necessary to increase the peak current of the RTM from the present value of approximately 100 mA to about 2 A. This must be accomplished without increasing the average current of the RTM, which is limited by the power available from the 500-kW CW klystron that drives the machine. We are planning to achieve this by replacing

the existing 100-keV thermionic gun and chopper-buncher system with a 110-keV photocathode gun. The frequency-doubled mode-locked Nd:YAG laser that excites the cesium-antimonide photocathode will provide ~ 70-ps light pulses at the 32nd subharmonic of the RF frequency. One watt of laser average power will be sufficient to obtain 12 pC per electron pulse. After time compression of the electron pulse in the buncher and the capture section of the injector linac, this should result in a 4-A pulse of 3-ps duration. The expected laser time jitter of 10 ps is reduced to less than 0.5 ps by the bunching process.

Much of the necessary photocathode-injector technology has been developed at Los Alamos, where peak currents of several hundred amperes have been observed with normalized brightness exceeding our requirements.[3] In the Los Alamos system, the photocathode is located in a high-field RF cavity because of the large space-charge forces at their high currents. This is not necessary for our relatively modest current requirement. The major remaining problems with the photocathode injector system are related to photocathode lifetime, stability, and reliability. If these problems prove to be serious, a pulsed thermionic gun with subharmonic bunching is a backup possibility for our system.

Because of the much higher peak current, the photocathode injector is expected to have larger emittances (both longitudinal and transverse) than our present system, but still well below what is needed to obtain the design values given in Table I.

Electron Beam Transport

Figure 1 is an overview of the entire FEL facility. The transport system extracts the electron beam from the RTM, carries it through a shielding wall into the FEL area, provides a beam waist at the center of the wiggler, and finally disposes of the beam in a shielded dump. The transport system is

achromatic and isochronous so that the small energy jitter and spread do not contribute to the positional or time jitter or beam size in the wiggler.

Coarse energy adjustment is made without changing any operating parameters of the RTM by moving the extraction magnet, D11 in figure 2, from one return leg to another. This provides energy steps of 12 MeV from 29-MeV minimum to 185-MeV maximum. The beam of the desired energy is deflected about 2° by D11, emerges from the end magnet E1 at 2° to the normal, and enters a spatially fixed extraction line. Different beam energies are transported by changing only the magnetic fields in the dipole (D) and quadrupole (Q) magnets in the extraction line.

The size and location of the beam waist at the wiggler is controlled by a variable telescope consisting of two quadrupole pairs (Q18-Q19 and Q20-Q21 in figure 3). The waist size must be adjustable to obtain optimal coupling to the optical mode in the cavity. The waist location must be adjustable because we use different wiggler lengths for long and short wavelength FEL operation. The half-length wiggler (HLW) consists of the first 65 periods of the 130 period full-length wiggler (FLW). Also shown in figure 3 is the four-dipole (D14, 15, 16, 17) achromatic chicane which guides the electron beam around the upstream optical cavity mirror.

The expected normalized transverse emittance of the beam is $\leq$ 10 μm. The normalized acceptance of the RTM is 63 μm, determined by the aperture of the 8-m long linac. The acceptance of the transport system must be larger than the RTM acceptance so that, barring gross missteering, there is no beam loss anywhere. This is especially important in the wiggler vacuum chamber where even minor beam impingement could result in serious damage to the permanent magnets and the optical components. At 29 MeV, using the HLW, the

calculated (normalized) extraction line acceptance is 81 μm and the vacuum chamber acceptance is 470 μm. At 185 MeV, using the FLW, the corresponding acceptances are 430 μm and 1730 μm.

FEL Physics

The performance of the NBS/NRL FEL has been analyzed using a fully three-dimensional (3-D) self-consistent computer code, SHERA, developed at NRL.[4] This analysis uses electron beam parameters close to the expected performance parameters of the RTM, and FEL parameters that optimize the power gain, G_p, in the 1-D small-signal low-gain limit:

$$G_p = 2 F_1^2 \frac{\pi^2}{\sigma_R} \frac{I}{I_A} \frac{\lambda_w^2}{\gamma^3} K^2 N^3 \frac{\delta}{\delta\nu} \left(\frac{\sin \nu}{\nu}\right)^2, \qquad (3)$$

where: $F_1 = J_0(b) - J_1(b)$, where J_0, J_1 are Bessel functions and

$b = K^2/2(1 + K^2)$,

$\sigma_R = \pi r_0^2$ is the cross-sectional area of the radiation, with r_0 the 1/e radius of an (assumed) gaussian radiation field amplitude,

I = electron beam peak current,

$I_A = 1.7 \times 10^4$ A is the Alfvén current,

λ_w = wiggler wavelength,

$K = |e B_w \lambda_w/2\pi mc^2|$, with B_w the RMS wiggler magnetic field and mc^2 the electron rest energy,

N = number of wiggler periods,

$\nu = -N\lambda(\omega - \omega_0)2c$ is the normalized frequency mismatch, and

$\omega_0 = 2\gamma^2 c(2\pi/\lambda_w)/(1 + K^2) = 2\ mc/\lambda$ is the resonant angular frequency.

Our wiggler design has a period λ_w = 28 mm and a maximum peak magnetic field of 0.54 Tesla, resulting in K = 1.0 as the maximum (RMS) wiggler parameter. Figure 4 is a plot of the 1-D power gain, from equation (3) (with $\frac{\delta}{\delta\nu}(\frac{\sin\nu}{\nu})^2$ = 0.54, its maximum value) for these wiggler parameters, and a peak current of 2 A. We use N = 130 or N = 65 respectively for shorter and longer optical wavelengths. The circles in figure 4 are point calculations at the indicated beam energies. The short curves are the result of varying K from 1.0 (at the circle) to 0.6 (by varying the wiggler magnetic field) while keeping the beam energy constant.

The 3-D calculations for our FEL are described in detail in reference 4. We summarize these results briefly here. Figure 5 compares the 1-D gain with the 3-D gain as a function of emittance, for a beam current of 2 A and γ = 350 (λ = 230 nm). The gain decreases only by about 30% for a factor of four increase in ε_n from its design value of 5 μm. Calculations of the type indicated in figure 5 were performed over the entire range of γ and K, with the results summarized in figure 6. At all but the shortest wavelengths, the decrease in gain due to degraded emittance is negligible. Figure 6 indicates that if we can achieve a peak current of 2 A or greater with $\varepsilon_n \leq$ 10 μm, we can expect to achieve lasing at wavelengths down to about 200 nm.

In similar calculations performed at different currents, we find that the gain per unit beam current increases as the current increases, as shown in figure 7 for the case γ = 150 (λ = 1.25 μm), and ε_n = 10 μm. (The curves in figure 7 are normalized to the 1-D maximum gain per unit current.) This is apparently due to the onset of the self-focussing or optical guiding phenomenon.[5] The guiding effect disappears at shorter wavelengths (for fixed ε_n): at λ = 230 nm the calculated 3-D gain is almost exactly proportional to beam

current in the range up to 4 A. The guiding effect can also be seen in a plot of the 1/e radius of the radiation as a function of axial distance in the wiggler. This is shown in figure 8, where L_w is the wiggler length and the optical cavity is adjusted to have a Rayleigh range of $L_w/2$ (in the absence of guiding). The beam travels left-to-right in figure 8. The guiding is quite pronounced at a current of 4 A.

Wiggler Design

Excellent magnetic field quality is needed in the wiggler to insure that we achieve close to the theoretical gain, especially at the shortest wavelengths where decreasing gain and decreasing mirror reflectivity combine to limit the minimum lasing wavelength. Good field quality is also important for obtaining high yields of spontaneous coherent radiation at the odd harmonics of the lasing frequency. There is strong interest among our prospective user community in the short wavelengths obtainable in this way.

The wiggler must be versatile for three reasons: to allow wavelength tuning by adjusting the wiggler field, to improve operation at long wavelengths where pulse slippage effects require a shorter wiggler, and to permit tapering of the wiggler to enhance power extraction efficiency. We choose to incorporate a 130 period FLW and a 65 period HLW in a single device because of the limited space in our existing building.

Although the average power of our FEL will be high even with an untapered 130 period wiggler by virtue of the high average power of our CW electron beam, the peak power in the micropulses is not very high. Tapering could improve the extraction efficiency and output power by an order of magnitude. In our CW system, we may be able to initiate lasing with the wiggler in an

untapered configuration for maximum small signal gain then adjust the taper to optimize output power.

Since a survey of potential vendors has convinced us that our wiggler requirements are within the state of the art, we have decided to obtain the wiggler commercially. Specifications of the wiggler are given in Table II. Tolerances on the magnetic field accuracy are given in Table III.

Table II Wiggler Specifications

Wavelength	28 mm
Number of Periods:	Full wiggler 130 + ends Half wiggler 65 + ends
Minimum Gap	10.0 mm
Peak Field at Minimum Gap	>0.54 Tesla
Permanent Magnet Material	(Any) SmCo alloy
Taper:	Adjustable 0 - 0.5 mm/m Independently adjustable, each half
Steering:	Both ends and every 33 periods
Vacuum Chamber:	8.4 x 16 mm^2 bore, pairs of ports every 33 periods

Table III Wiggler Tolerances

RMS field error < 27 gauss (0.5% $B_{0\ max}$)

Integral field errors (both planes)

$$\left| \int_{33\ periods} Bdz \right| < 23 \text{ gauss cm}$$

Third harmonic amplitude < 0.1 B_0

Transverse field variation < 0.5% B_0 for $|x| < 5$ mm

Optical Cavity

Figure 9 is a schematic view of the optical cavity with the apertures shown. We choose to make the cavity symmetric about the wiggler center in the FLW case, with a cavity length of 8.062 m. Since the photocathode is to operate on the 32nd subharmonic of the RF frequency, there will be four independent light pulses in the cavity at all times. When we convert to the HLW configuration, we will keep the cavity mirror locations fixed and remove the downstream wiggler half. We want the waist location at the center of the wiggler, and a Rayleigh length of half the wiggler length in both cases. This leads to the parameter sets listed in Table IV.

Mirror sizes and all apertures, except for the wiggler vacuum chamber, can be chosen so that diffraction losses are negligible at all wavelengths. The aperture of the wiggler chamber is constrained by the magnetic field and wiggler period. Modelling the ends of the chamber as discrete apertures, the diffraction loss, D, at each encounter of the light pulse with the chamber end is negligible at short wavelengths, increasing to a maximum of 0.6% at λ = 10 μm.

The intra cavity power is given by

$$P_{cav} = q\eta P_B, \tag{4}$$

where $q = \dfrac{(1 - D)^3 R_{HR} R_{OC}}{1 - R_{HR} R_{OC} (1 - D)^4}$,

P_B is the electron beam power,

R_{HR} is the reflectivity of the upstream (high reflectivity) mirror,

R_{OC} is the relfectivity of the downstream (output coupler) mirror, and

η is the extraction efficiency of the wiggler.

Assuming that output coupling is accomplished with a partially transmitting downstream mirror with transmission T, the output power is given by

$$P_{out} = T\,P_{cav} = qTnP_B \qquad (5)$$

If the two cavity mirrors have the same absorption, A, and scattering, S, losses,

$$R_{OC} = R_{HR} - T. \qquad (6)$$

In order to achieve lasing, $G_p > 1/q$ is required. However, large q means that P_{cav} is large and thus mirror damage is a very serious concern, especially at short wavelengths where G_p is small, damage-threshhold fluence is low, and mode size at the mirror is small.

Table IV Optical Cavity Geometric Parameters

Parameter	FLW	HLW
Optical wavelength, λ (μm)	0.2 to 2.0	2.0 to 10.0
Mirror separation, L (m)	8.06158	8.06158
Rayleigh length, Z_0 (m)	1.82	0.91
Cavity waist to downstream mirror distance (m)	4.03079	4.94079
Downstream mirror radius (m)	4.85256	5.10839
Upstream mirror radius (m)	4.85256	3.38614
Minimum waist, $r_0(\lambda_{min})$ (mm)	0.340	0.761
TEM_{00} (1/e) radius on mirror in units of r_0		
Downstream	2.430	5.521
Upstream	2.430	3.572

Predicted Performance

We can predict the laser output power and fluence with reasonable confidence for the design of accelerator, wiggler, and optical cavity described above. The electron beam average power is given by

$$\langle P_B \rangle = f_i \cdot I \cdot \Delta t \cdot \gamma mc^2, \qquad (7)$$

where f_i = 74.375 MHz (the 32nd subharmonic of the RF frequency), I = 2 A and Δt = 3 ps. In terms of accelerator capability, these parameters give conservative values of $\langle P_B \rangle$. Even at the design maximum energy, γmc^2 = 185 MeV, equation (7) gives $\langle P_B \rangle$ = 83 kW, whereas the RTM should be capable of producing > 100 kW of beam at all energies up to the maximum. Since none of the parameters (74.375 MHz, 2 A, or 3 ps) are necessarily maxima, more beam power may in fact be available.

When the laser reaches equilibrium, the power entering the cavity per pass, ηP_B, must equal the power loss per pass P_{cav}/q. We estimate $\eta = \frac{1}{2N}$, which is the extraction efficiency of a perfect, untapered, N-period wiggler. We ignore both wiggler field errors which would decrease η, and the possibility of tapering the wiggler which could substantially increase η. Then from equation (7), with the aid of the FEL resonance condition

$$\lambda = \frac{\lambda_w}{2\gamma^2}(1 + K^2), \tag{8}$$

we obtain (for K = 1)

$$\eta\langle P_B \rangle \text{ (kW)} = 0.147/\sqrt{\lambda(\mu m)} \text{ (FLW)}$$

$$\eta\langle P_B \rangle \text{ (kW)} = 0.293/\sqrt{\lambda(\mu m)} \text{ (HLW)} \tag{9}$$

For each wavelength of interest we choose a value of R_{HR} appropriate for commercially available multi-layer dielectrics, and values of T for which G_ρ exceeds 1/q by at least 3%, and calculate $\langle P_{out} \rangle$ using equations 4-7. Figure 10 shows the estimated average output power of the FEL as a function of wavelength. The predicted output fluence and peak irradiance, corresponding to the values in figure 10, are shown in figure 11.

The spectral bandwidth, $\Delta\nu$, should be given by the Fourier-transform limit. If the temporal pulse shape were a 3 ps (FWHM) Lorentzian,

$$\Delta\nu = \frac{\ell n\ 2}{\pi} \cdot \frac{1}{\Delta t_{FWHM}} = 74\ \text{GHz}. \qquad (10)$$

Thus the fractional resolution $\Delta\nu/\nu$ would be in the range 2.5×10^{-3} (at 10 μm) to 5×10^{-5} (at 200 nm).

Thus far we have concentrated on the performance of a "conventional" fundamental wavelength CW FEL. There are several very important extensions that may be implemented as the project develops. These include:

1. Third-harmonic lasing which might extend the short wavelength limit to about 150 nm.
2. Utilization of spontaneous coherent harmonic (non-lasing) light. With our expected excellent electron beam quality and minimization of wiggler errors, significant intensity of narrow-band light is expected at the odd harmonics of the laser frequency down to perhaps 25 nm or less.
3. A cavity-dumped mode of operation which might, under favorable conditions, increase the peak power by close to two orders of magnitude.
4. Output pulse shortening with the goal of obtaining pulse lengths of order 100 fs or less, at high peak power levels.

Table V Design Outcoupling Fractions and Assumed Reflectivities

	λ, μm	T	R_{HR}
	200 nm	0.005	0.975
	250 nm	0.005	0.980
	300 nm	0.010	0.985
FLW	350 nm	0.010	0.995
	400 nm	0.010	0.999
	600 nm	0.010	0.999
	1.0 μm	0.010	0.999
	2.0 μm	0.010	0.999
	2.0 μm	0.030	0.990
	3.0 μm	0.030	0.990
HLW	4.0 μm	0.030	0.990
	5.0 μm	0.030	0.990
	10.0 μm	0.010	0.990

References

1. S. Penner et al., IEEE Trans. on Nucl. Science NS-32, No. 5, 2669 (1985).

2. M.A. Wilson et al., Proc. 1987 IEEE Particle Accelerator Conf., IEEE Catalog No. 87CH2387-9, p 322.

3. J.S. Fraser et al., Proc. 1987 IEEE Particle Accelerator Conf., IEEE Catalog No. 87CH2387-9, p 1705.

4. C.M. Tang et al., "Analysis of Free Electron Laser Performance Utilizing the National Bureau of Standards' CW Microtron," to be published in J. Appl. Physics.

5. P. Sprangle, A. Ting, and C.M. Tang, Phys. Rev. Lett. 59, 202 (1987). P. Sprangle, A. Ting, and C.M. Tang, Phys. Rev. A36, 2773 (1987).

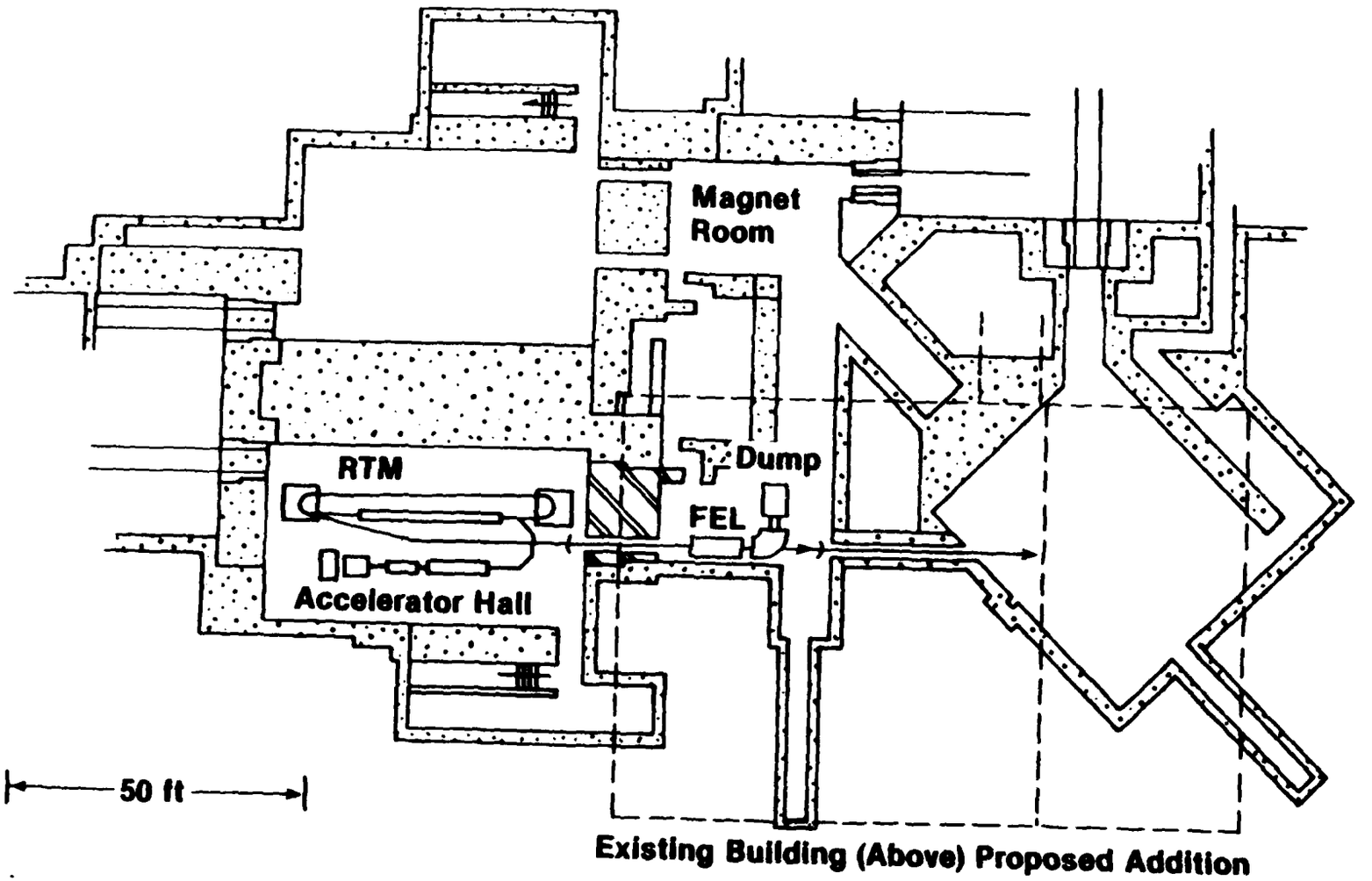

Figure 1 Plan view of NBS FEL facility.

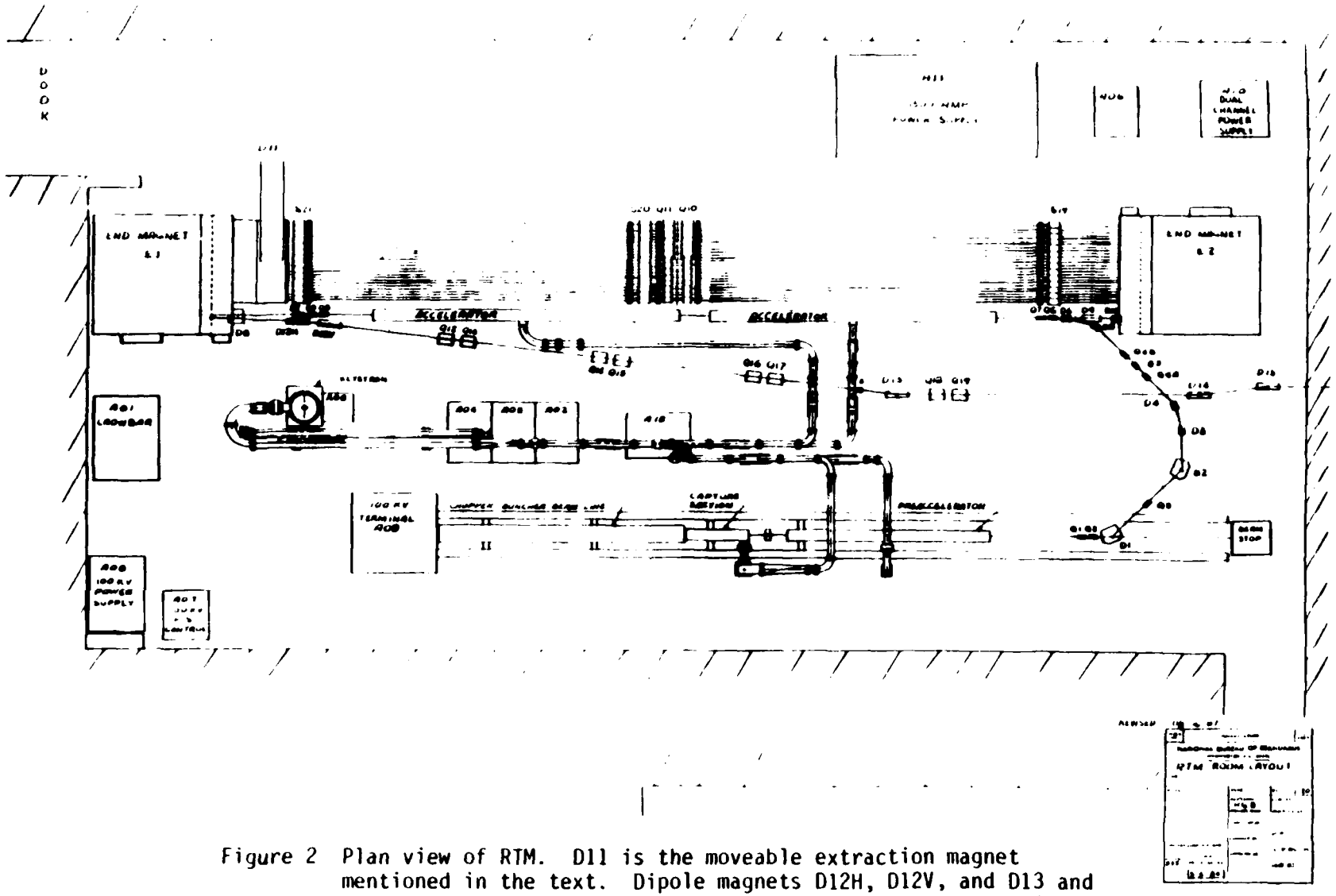

Figure 2 Plan view of RTM. D11 is the moveable extraction magnet mentioned in the text. Dipole magnets D12H, D12V, and D13 and quadrupole magnets Q12 through Q17 constitute the extraction line.

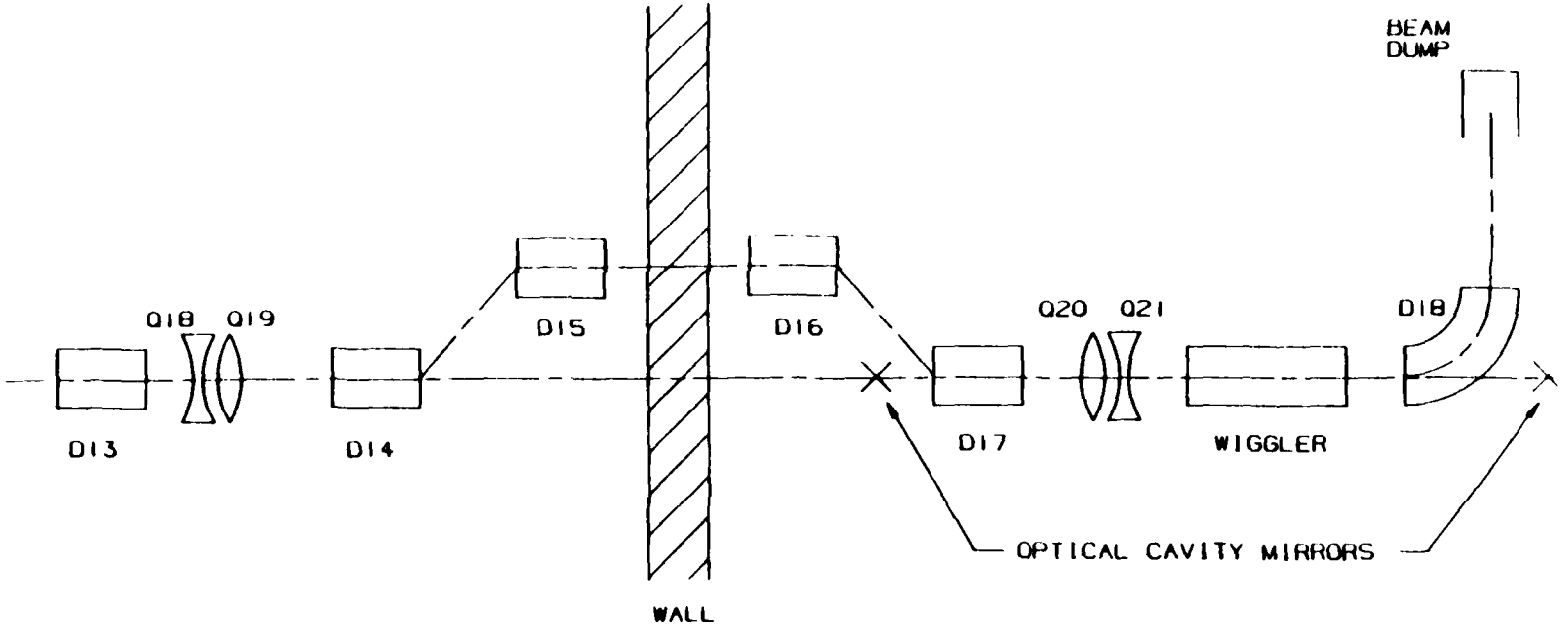

Figure 3 Schematic view of electron beam transport line through the wiggler.

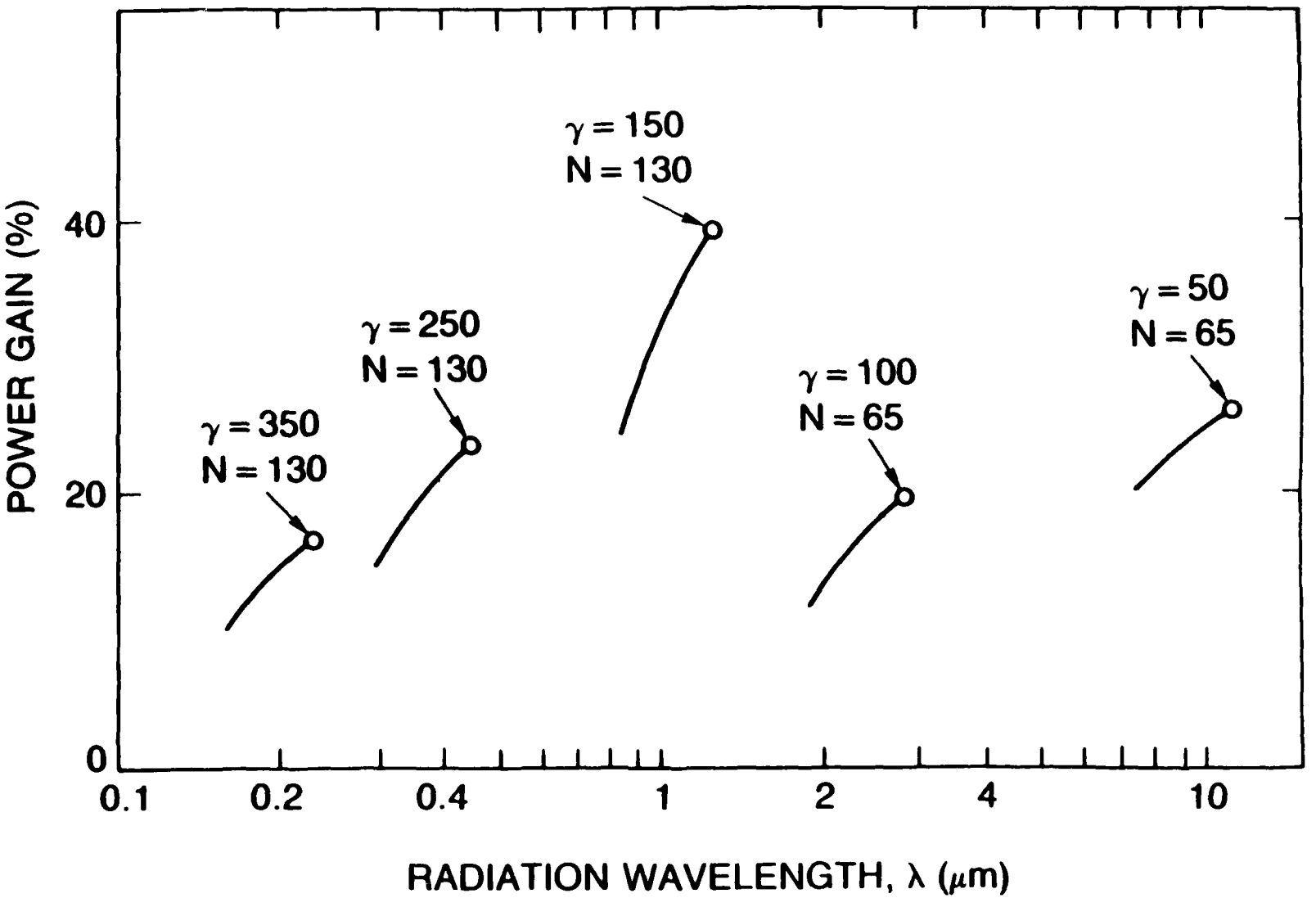

Figure 4 Power gain as a function of radiation wavelength from the 1-D calculation with I = 2 A.

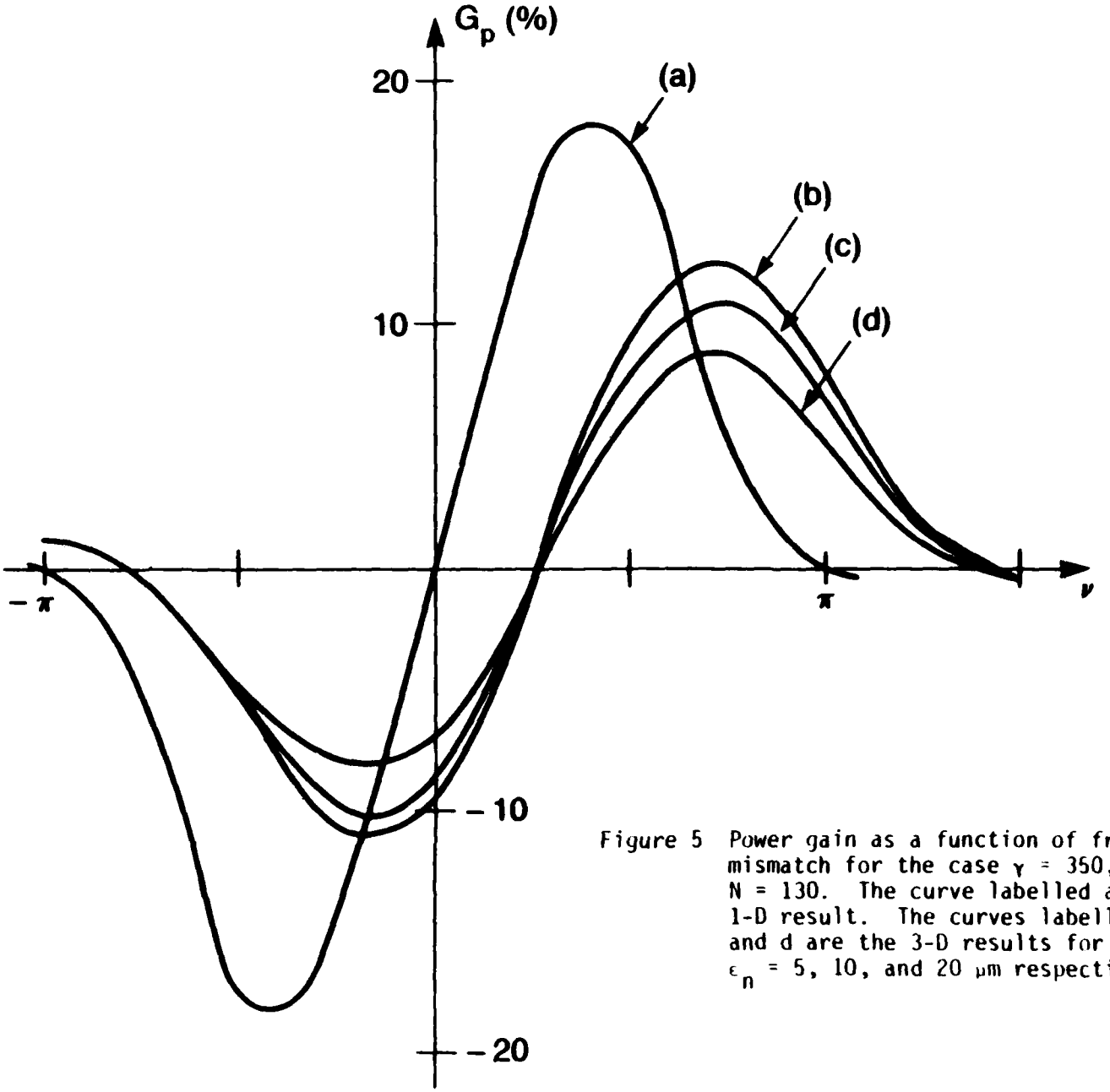

Figure 5 Power gain as a function of frequency mismatch for the case γ = 350, I = 2 A, N = 130. The curve labelled a is the 1-D result. The curves labelled b, c, and d are the 3-D results for the cases ϵ_n = 5, 10, and 20 μm respectively.

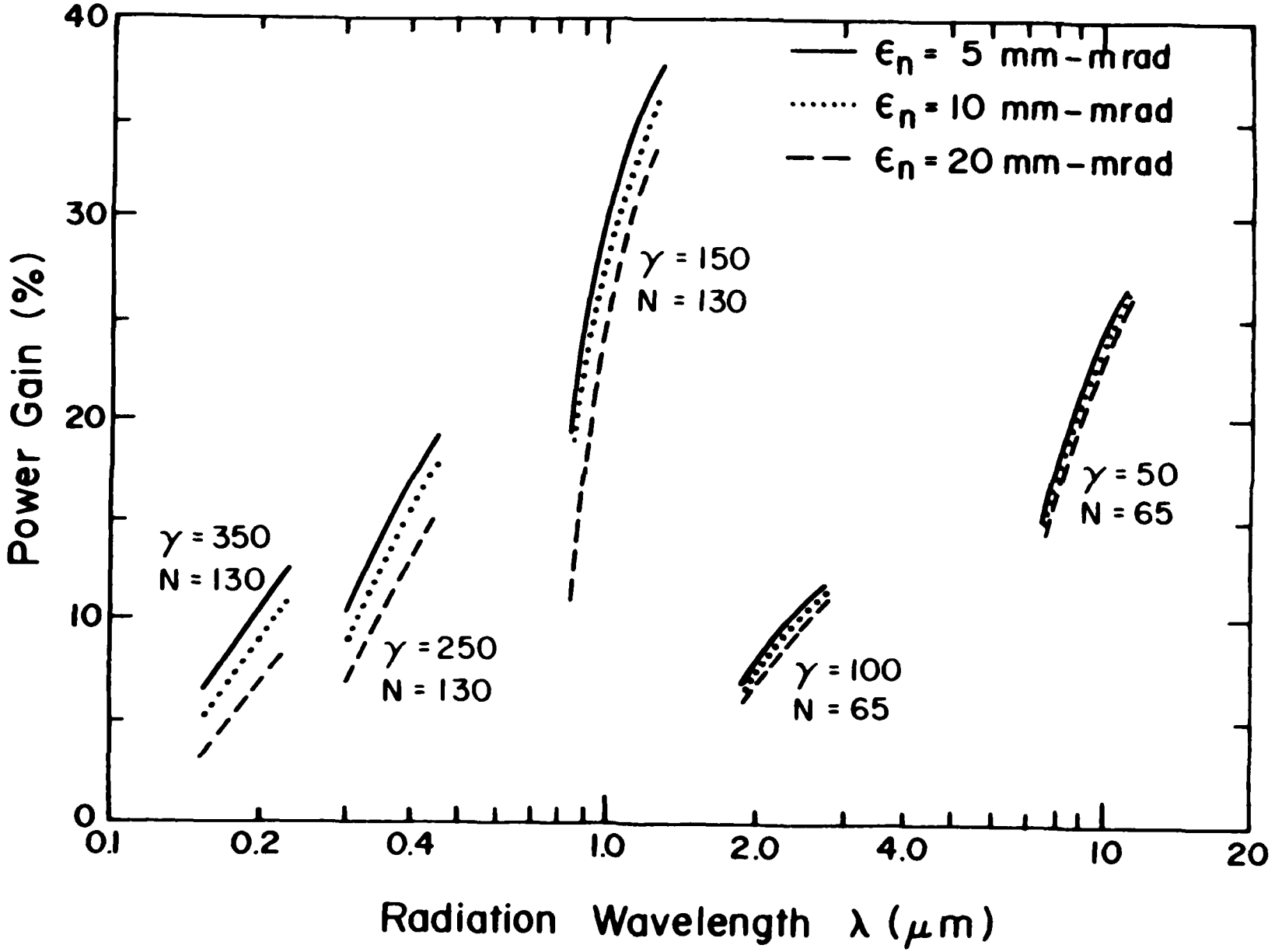

Figure 6 Power gain as a function of radiation wavelength from the 3-D calculations with I = 2 A.

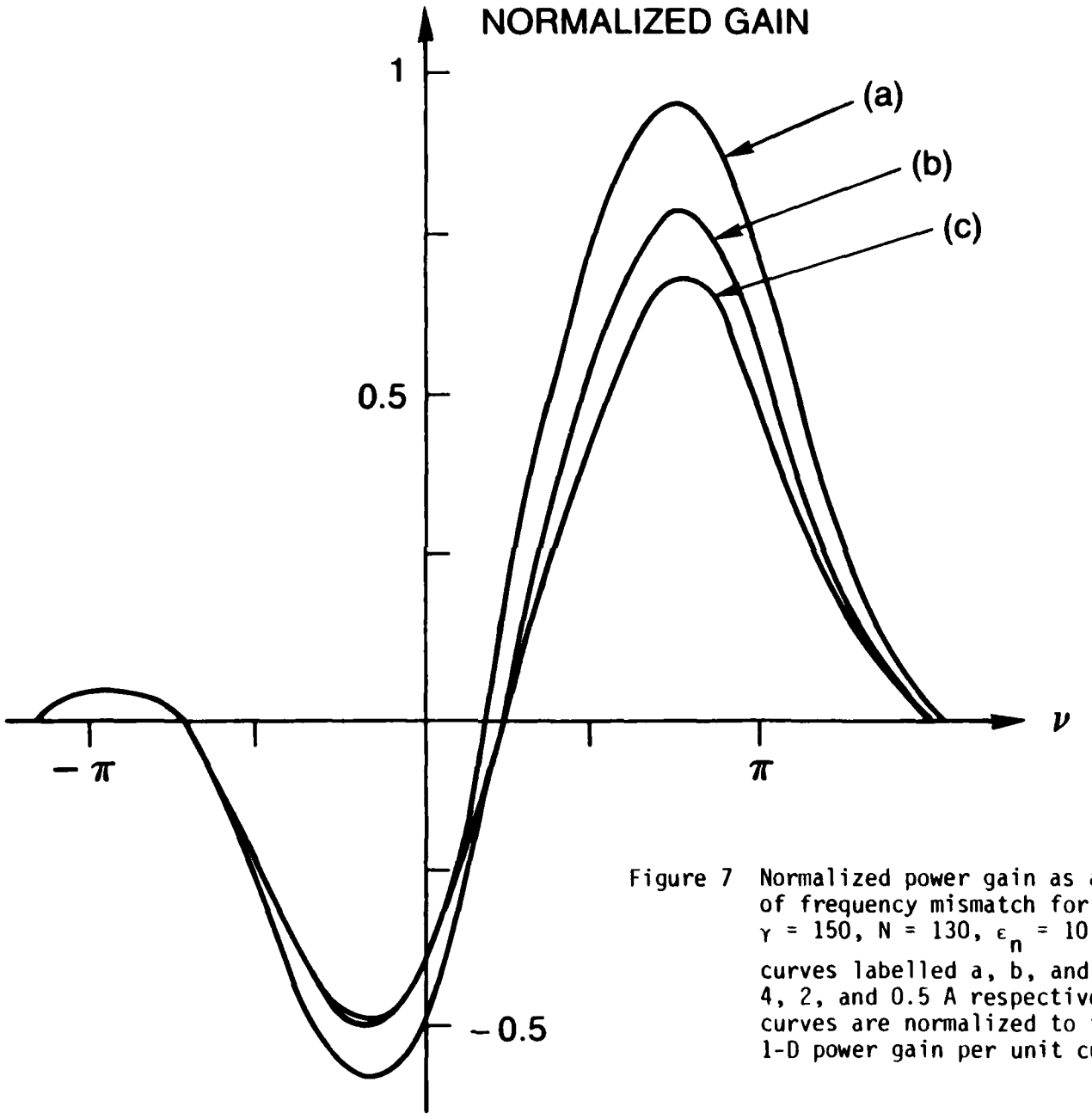

Figure 7 Normalized power gain as a function of frequency mismatch for the case $\gamma = 150$, $N = 130$, $\epsilon_n = 10$ μm. The curves labelled a, b, and c are for 4, 2, and 0.5 A respectively. The curves are normalized to the maximum 1-D power gain per unit current.

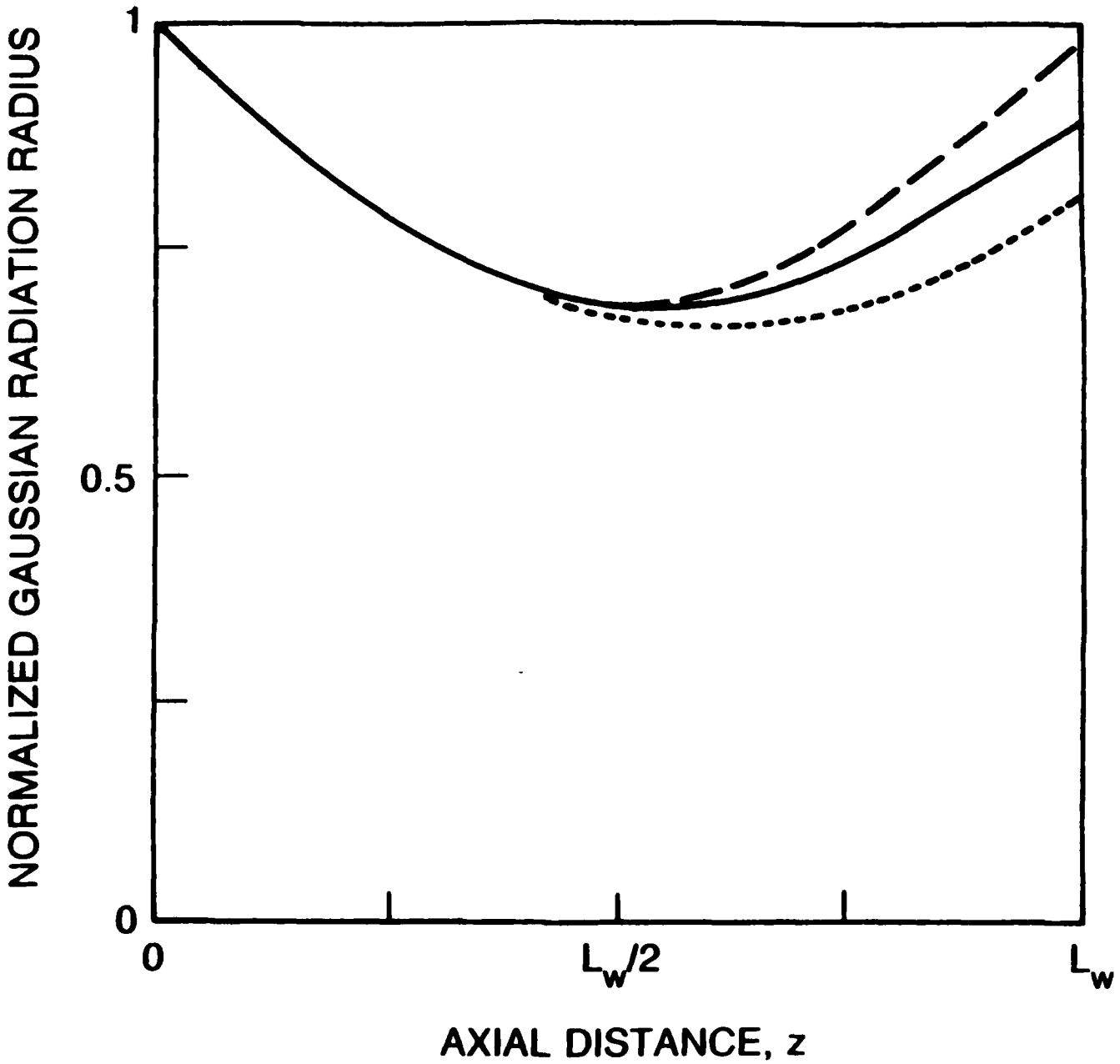

Figure 8 Relative 1/e size of the radiation amplitude as a function of axial distance. The parameters of the calculation are the same as in figure 7. Long-dashed curve - 0.5 A; solid curve - 2 A; short-dashed curve - 4 A.

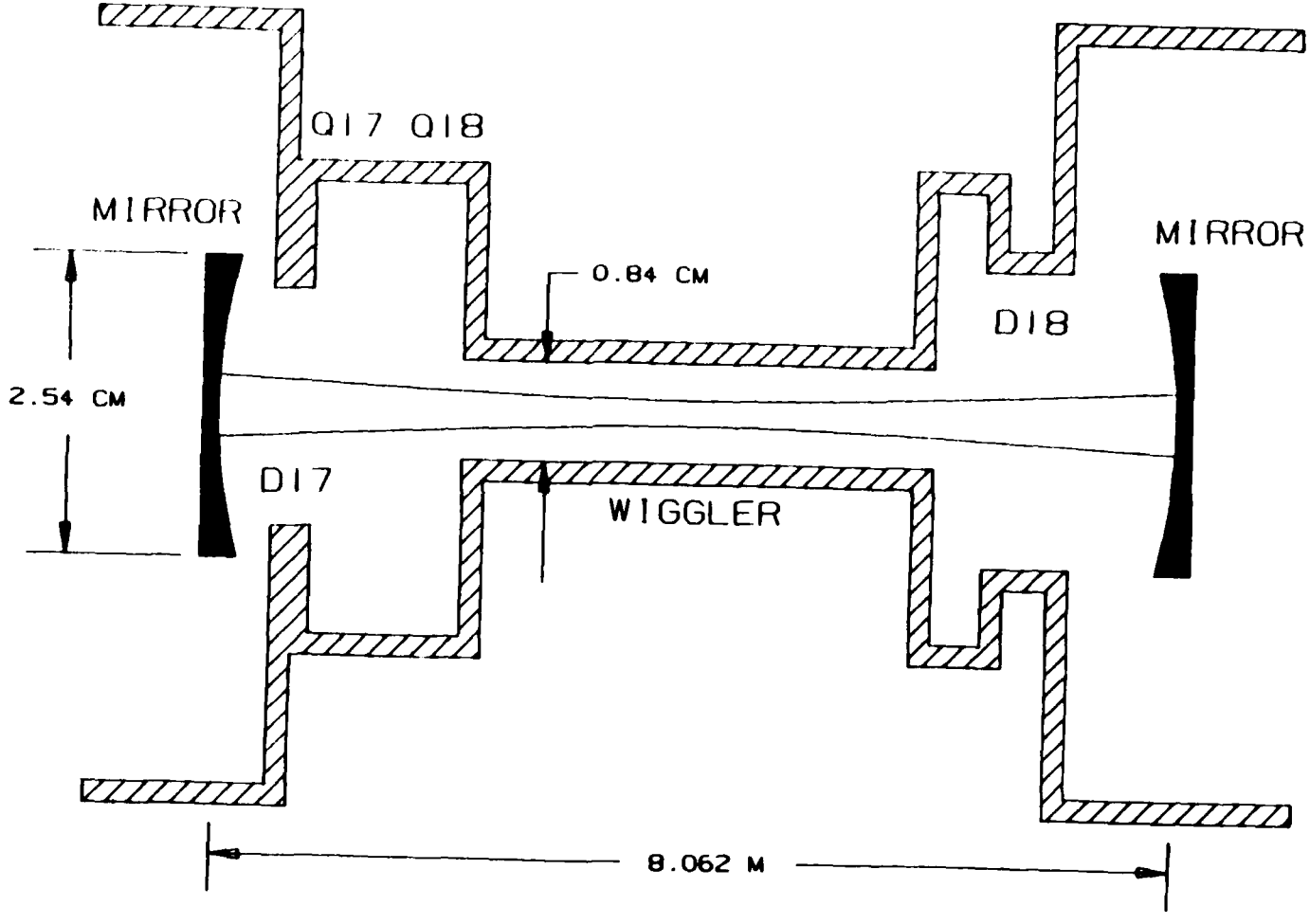

OPTICAL RESONATOR FOR THE FULL LENGTH WIGGLER

Figure 9 Optical resonator layout for the full length wiggler. The vacuum envelope is indicated by the shaded regions. The transverse scale is magnified 100 times compared to the longitudinal scale.

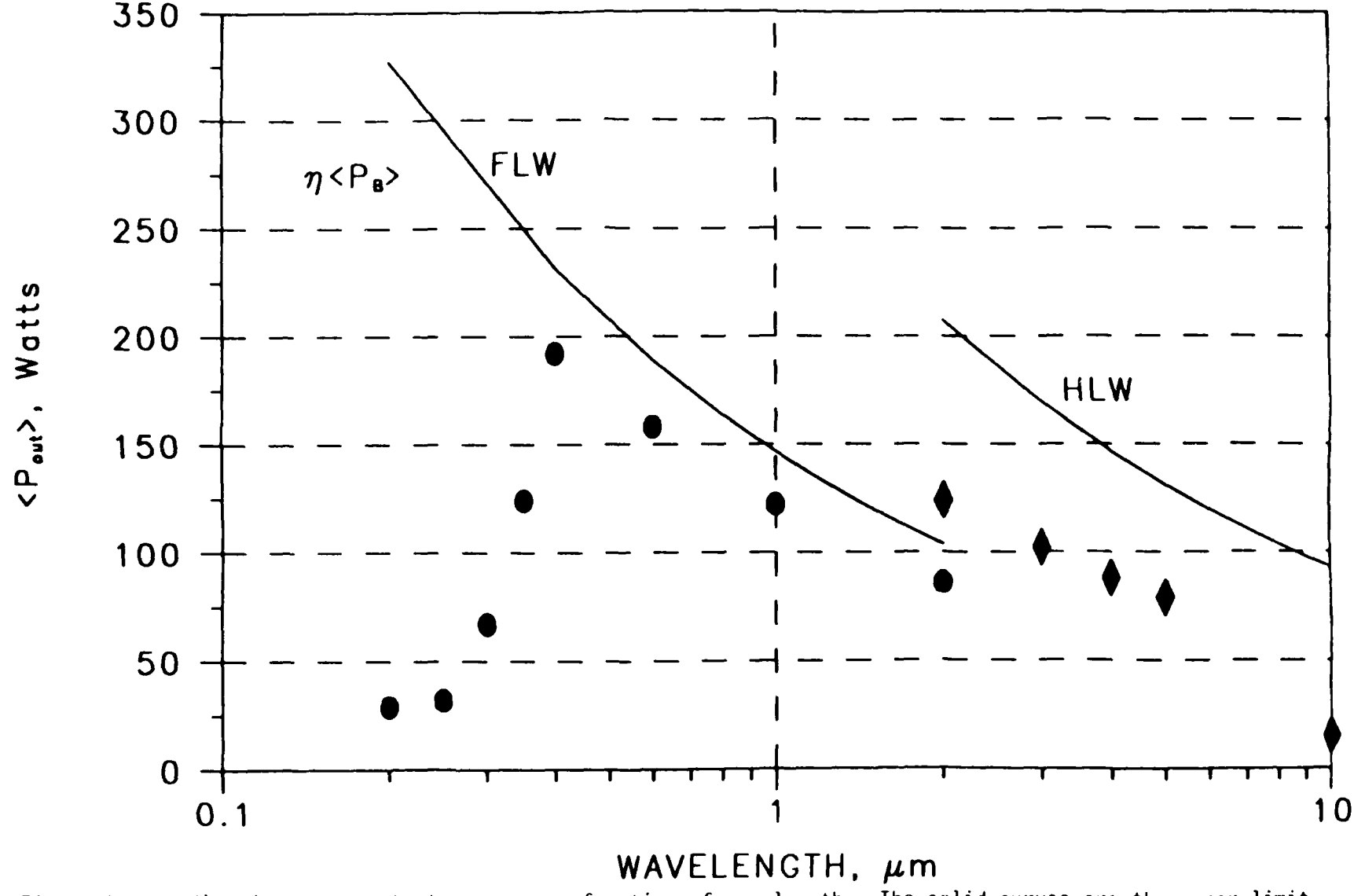

Figure 10 Predicted average output power as a function of wavelength. The solid curves are the upper limit, $\langle P_B\rangle/2N$, for the case R_{HR} = 1.0, D = 0. The circles (for the FLW) and diamonds (for the HLW) are calculated values of output power using the values of R_{HR} and T given in Table V, and calculated values of D.

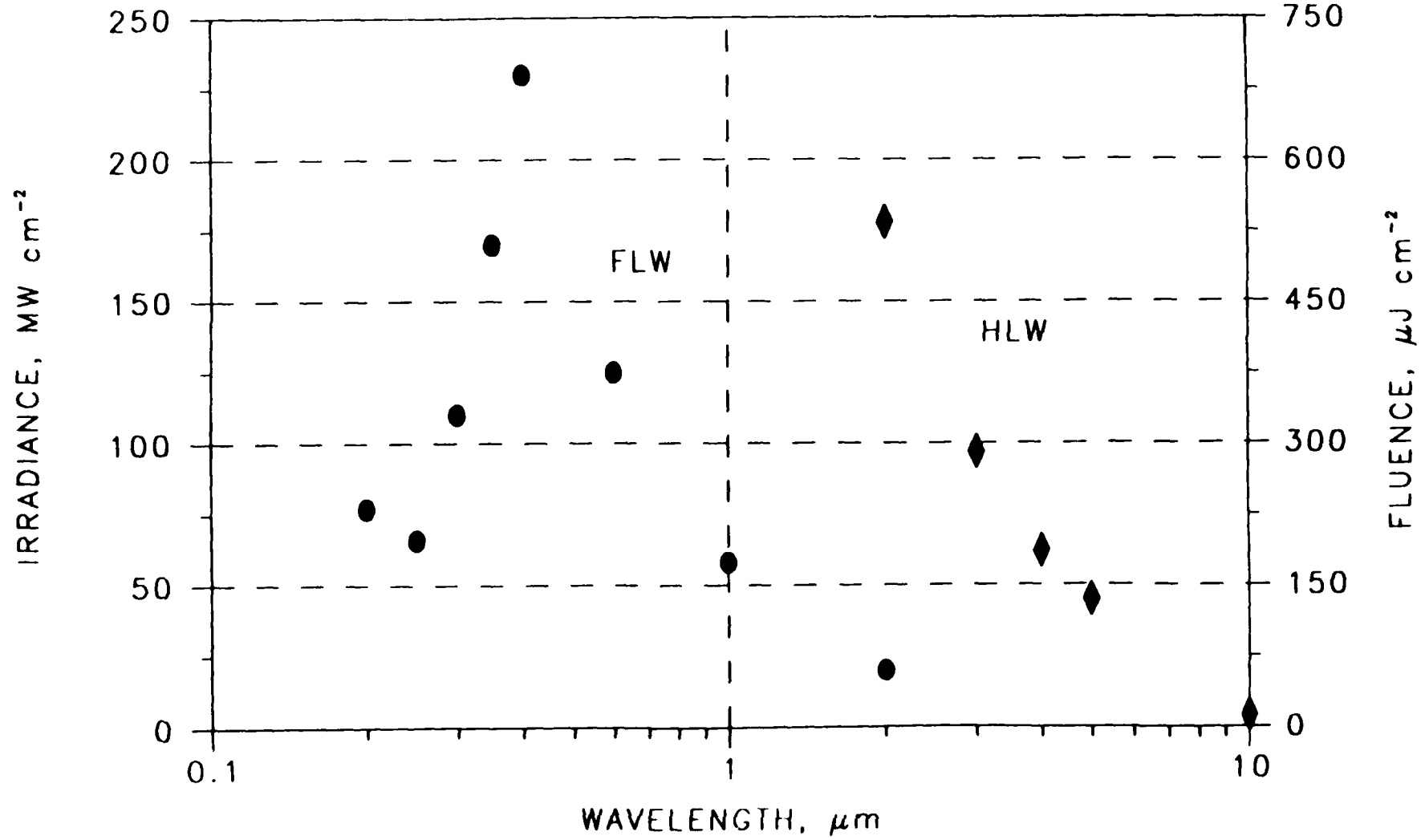

Figure 11 Predicted output fluence per micropulse and peak irradiance as a function of wavelength, corresponding to the average power in figure 10. The mode areas used to obtain the values in figure 11 are the beam 1/e (amplitude) size corrected for the defocussing of the output coupler.

END

DATE

FILMED

8-88

DTIC